JOURNAL OF MATERIALS SCIENCE 26 (1991) 2143–2149

Computer modelling of the origin of defects in ceramic injection moulding

Part III *Sprue closure*

K. N. HUNT, J. R. G. EVANS
Department of Materials Technology, Brunel University, Uxbridge, Middlesex, UB8 3PH, UK
J. WOODTHORPE
T & N Technology, Cawston House, Cawston, Rugby, CV22 7SA, UK

A finite difference method for the calculation of sprue closure time is described and compared with measured cavity pressure fall for a zirconia–polystyrene suspension. The disparity between measured and calculated values is explained by the balance of volume shrinkage rate in the cavity and flow rate in the sprue during the final stage of mould packing and cooling.

1. Introduction

The injection moulding of large ceramic bodies suffers from two major difficulties: (i) the control of solidification in the cavity and (ii) the removal of the organic vehicle. Previous work has shown that defects are initiated in large sections during solidification in wax-based [1] and high polymer-based [2] organic vehicles. A number of methods for the control of solidification have been reviewed [3] and one of them, the use of modulated hold pressure, has been described in detail [4–8]. The present work is part of a study [9, 10] to describe the solidification stage of ceramic injection moulding by a numerical model. This facility permits the exploration of the effects of a large number of material and machine parameters on the incidence of defects. In the first instance, static hold-pressure moulding is considered. The initial objective is to validate computer models by appeal to experiment and to account for disparities.

A crucial stage in solidification is the time at which the sprue closes and the molten core of the moulded body is disconnected from the hold pressure. In previous work [8] a good correlation was found between calculated sprue solidification time and the time to cavity pressure drop, in agreement with general statements in the literature [11, 12]. However, that work used a semicrystalline polymer blend with a high melting point, namely 158 °C, so that flow in the sprue was interrupted well above T_g by the sudden onset of crystallization and any discrepancy was small. The present study uses an amorphous polymer whose glass transition temperature has been lowered to 58 °C by the addition of a diluent. The time at which the cavity pressure began to fall was found to be significantly less than the calculated sprue solidification time [10].

Few studies have attempted to quantify the flow of material during the packing and cooling stages of injection moulding. In work by Kamal *et al.* [13, 14] the packing stage was regarded as the compression of material in the mould until a maximum pressure was reached and flow stopped. Cooling then occurred without additional packing. A more recent study by Huilier *et al.* [15] has stated that this assumption is not valid and matter continues to enter the mould as long as a pressure gradient exists or gate sealing is incomplete. They attempted to validate their model by injection-moulding polystyrene at 30 MPa into a flat rectangular plate. The cavity pressure was found experimentally to fall considerably sooner than predicted by their model and this discrepancy was left unexplained. Flow through the sprue bush was not considered.

In fact, the final stage of mould packing and cooling involves a competition between shrinkage of the core of the moulding as temperature falls and the non-isothermal flow at low shear rates along the shrinking core of the sprue. Thus the condition

$$\left(\frac{dV}{dt}\right)_{\text{shrinkage}} > \left(\frac{dV}{dt}\right)_{\text{flow}} \quad (1)$$

defines the time at which flow in the sprue ceases to compensate for shrinkage in the core and cavity pressure thereafter falls. Viewed in this light, sprue closure is seen not as an instantaneous event, but as part of a dynamic process which is influenced by material properties, mould design and machine settings.

In previous work [2] it has been argued that a low temperature-dependence of viscosity of the suspension is one of a set of material properties that is desirable for the avoidance of shrinkage-related defects. The argument is simply that resistance to flow along the constricted sprue, runner and gate channels as temperature falls should be as small as possible. The present work attempts to present a quantitative basis for this assertion, and shows why an exact time of sprue closure cannot be obtained for use in the computer modelling of shrinkage-related defects.

0022–2461/91 $03.00 + .12

2. Experimental details

2.1. Preparation of suspension

Zirconia (HSY3.0 from Daiichi-kigenso) was loaded at 45 vol % in a polystyrene (HF555, BP Chemicals) and dibutyl phthalate blend of weight ratio 5:1. Mixing was achieved by pre-blending in a Henschel high-speed mixer and subsequent twin-screw extrusion using a procedure previously described [16].

2.2. Injection moulding

The rectangular bar shown in Fig. 1 was moulded on a Sandretto 6GV 50 tonne machine using the conditions given in Table I. The sprue diameter at the smaller end is given and the sprue semi-angles were 2.1 and 1.6° for the large and small sprues, respectively. A Dynisco FT444DH force transducer was incorporated in the cavity adjacent to the sprue in the fixed mould half and pressure was recorded on a chart.

2.3. Viscosity measurement

A Davenport capillary rheometer was used to measure viscosity at temperatures of 112, 127, 142 and 162 °C and at shear rates of 0.45 to 5.80 s^{-1}, using a 5 mm diameter die 25 mm in length. Shear stress values for shear rates down to 0.26 s^{-1} were obtained by short extrapolation.

3. Computing

3.1. Calculation of sprue solidification time

The sprue solidification was modelled by assuming the sprue to be an infinitely long cylinder. For a general point in a cylinder, the heat transfer equation expressed in polar co-ordinates is

$$\frac{1}{\alpha}\frac{\partial T}{\partial t} = \frac{\partial^2 T}{\partial r^2} + \frac{1}{r}\frac{\partial T}{\partial r} \tag{2}$$

where α is thermal diffusivity and r is the radius. Using a forward difference representation for time and a centred difference representation for space, this can be written in the pure implicit form as

$$\frac{1}{\alpha}\left[\frac{T(r, t+\Delta t) - T(r, t)}{\Delta t}\right] = \left[\frac{T(r+\Delta r, t+\Delta t) - 2T(r, t+\Delta t) + T(r-\Delta r, t+\Delta t)}{(\Delta r)^2}\right] + \frac{1}{r}\left[\frac{T(r+\Delta r, t+\Delta t) - T(r-\Delta r, t+\Delta t)}{2\Delta r}\right] \tag{3}$$

Energy balance equations were written for the nodes at $r = 0$, the centre line and $r = n$, the material–sprue bush interface by reference to Fig. 2 as follows. For area 1 at $r = 0$

$$\rho C\pi\left(\frac{\Delta r}{2}\right)^2 \frac{\partial T(0, t)}{\partial t}$$

Heat stored

$$= k2\pi\left(\frac{\Delta r}{2}\right)\frac{\partial T[0 + (\Delta r/2), t + \Delta t]}{\partial r} \tag{4}$$

Conduction out of area

where ρ is the density, C the specific heat and k the themal conductivity of the composite.

For area 2 at $r = n$

$$\rho C\left[\pi r^2 - \pi\left(r - \frac{\Delta r}{2}\right)^2\right]\frac{\partial T(n, t)}{\partial t} =$$

Heat stored

$$- k2\pi\left(r - \frac{\Delta r}{2}\right)\frac{\partial T[n - (\Delta r/2), t + \Delta t]}{\partial r}$$

Conduction into area

$$- 2\pi rh[T(n, t + \Delta t) - T_m] \tag{5}$$

Heat flow out to sprue bush

where n is the surface heat transfer coefficient and T_m is the mould temperature.

Equations 3, 4 and 5 can be rewritten as

$$\left(-2a + \frac{a}{i}\right)T(i-1, t+\Delta t) + (1+4a)T(i, t+\Delta t) + \left(-2a - \frac{a}{i}\right)\times + T(i+1, t+\Delta t) = T(i, t) \tag{6}$$

$$(1+8a)T(0, t+\Delta t) - 8aT(1, t+\Delta t) = T(0, t) \tag{7}$$

and

$$-8a\left(\frac{2n-1}{4n-1}\right)T(n-1, t+\Delta t) + \left[1 + 8a\left(\frac{2n-1}{4n-1}\right) + 8b\left(\frac{n}{4n-1}\right)\right] \times T(n, t+\Delta t) = T(n, t) + 8b\left(\frac{n}{4n-1}\right)T_m \tag{8}$$

where

$$a = \frac{k\Delta t}{2\rho C(\Delta r)^2} = \frac{\alpha\Delta t}{2(\Delta r)^2} \qquad b = \frac{h\Delta t}{\rho C\Delta r}$$

These equations were solved after each time step Δt using the following algorithm for tridiagonal matrices:

$$\left|\begin{array}{rl|l} & & t+\Delta t \\ b_0T_0 + C_0T_1 & & = d_0 \\ a_1T_0 + b_1T_1 + C_1T_2 & & = d_1 \\ a_2T_1 + b_2T_2 + C_2T_3 & & = d_2 \\ a_iT_{i-1} + b_iT_i + C_iT_{i+1} & & = d_i \\ a_nT_{n-1} + b_nT_n & & = d_n \end{array}\right| \quad t \tag{9}$$

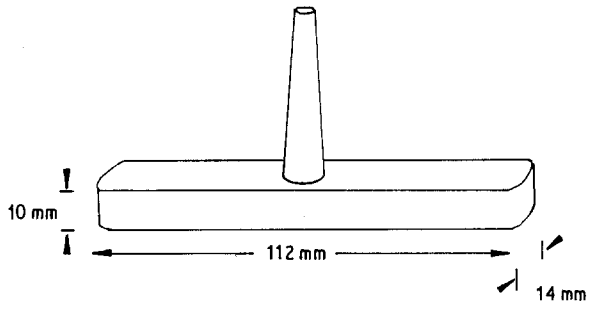

Figure 1 Dimensions of the moulded rectangular bars.

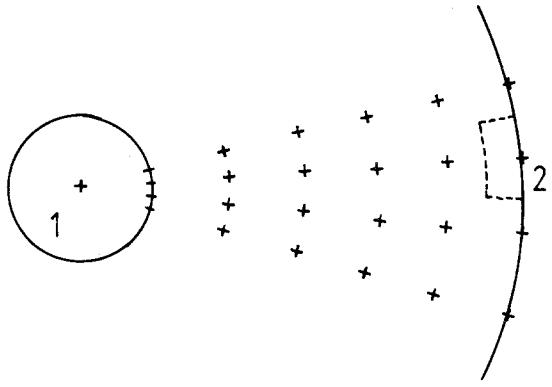

Figure 2 Finite difference mesh used for the calculation of sprue solidification.

which can be rewritten as

$$\begin{vmatrix} b_0 & C_0 & & & & \\ a_1 & b_1 & C_1 & & & \\ & a_2 & b_2 & C_2 & & \\ & & a_i & b_i & C_i & \\ & & & a_n & b_n & \end{vmatrix} \begin{vmatrix} T_0 \\ T_1 \\ T_2 \\ T_i \\ T_n \end{vmatrix}^{t+\Delta t} = \begin{vmatrix} d_0 \\ d_1 \\ d_2 \\ d_i \\ d_n \end{vmatrix}^{t} \quad (10)$$

The matrices on the right-hand side contain terms of temperature at time t while those on the left contain temperature at time $(t + \Delta t)$. These were solved at each time-step by Gaussian elimination using a simple algorithm [17]:

$$T_n = G_n$$
$$T_i = G_i - \frac{C_i T_{i+1}}{F_i} \quad (11)$$

where i is varied from $(n - 1)$ to 1 and the terms F and G are first calculated from

$$F_0 = b_0 \qquad G_0 = \frac{d_0}{F_0}$$
$$F_i = b_i - \frac{a_i C_{i-1}}{F_{i-1}} \qquad G_i = \frac{d_i - a_i G_{i-1}}{F_i} \quad (12)$$

where i is varied from 1 to n.

The sprue was taken to be solid when $T(0) = T_g$. This initial criterion for sprue closure was later modified to consider a more realistic point based on the balance of flow and shrinkage.

TABLE I Injection moulding conditions for rectangular bars

Screw rotation speed	150 r.p.m.
Dose stop position	9.0×10^{-5} m^3
Decompression stop position	9.5×10^{-5} m^3
Feed zone temperature	190 °C
Mid zone temperature	200 °C
Metering zone temperature	210 °C
Nozzle temperature	220 °C
Nominal injection speed	1.44×10^{-4} m^3 s^{-1}
Total injection time	90 s
Mould temperature	25 °C
Minimum sprue diameter	6.9 mm, 10 mm
Injection and hold pressure	10 to 100 MPa

3.2. Temperature distribution in the core of the moulding

For the rectangular bar shown in Fig. 1 the temperature distributions were calculated by a two-dimensional unsteady state finite difference method which has been described elsewhere [10].

3.3. Shrinkage of the core of the bar

The rate of shrinkage of the core of the moulding was calculated at time t for fixed intervals of 5 s after mould filling, assuming that the injection pressure was maintained constant. From the temperature distributions calculated in Section 3.2, the number of nodes of the finite difference mesh which were still molten at time $(t - 0.5)$ s was found. Uniform two-dimensional heat flow was assumed along the complete length of the bar so that end-effects were neglected. The volume of each element was taken to be $\Delta x \Delta y Z$ where Z was the length of the cavity. Using the temperature distribution and equation of state [9], the mass of material contained in the molten core at $(t - 0.5)$ s was calculated. A new temperature distribution was obtained for $(t + 0.5)$ s. The volume of the elements was assumed constant and a new mass was calculated for the same elements at $(t - 0.5)$ s regardless of whether they had solidified or not. The difference in the two masses gives a good approximation to the mass of material that must have flowed into the core of the moulding in a one-second interval centred on time t in order to maintain a constant hold pressure.

3.4. Calculation of predicted cavity pressure decay curve

The procedure for calculating the residual pressure in the molten core of the rectangular bar has been described [10]. Using this procedure, the residual pressure was calculated for each time step Δt in order to predict the decay of pressure in the cavity. The starting time for the calculation was taken as the experimental cavity pressure fall time, and the finishing time was taken as the time when the temperature of the centre of the core of moulding reached T_g. The method used the average specific volume in the molten core at the time when the cavity pressure drop occurred and the equation of state to calculate the subsequent pressures in the moulding.

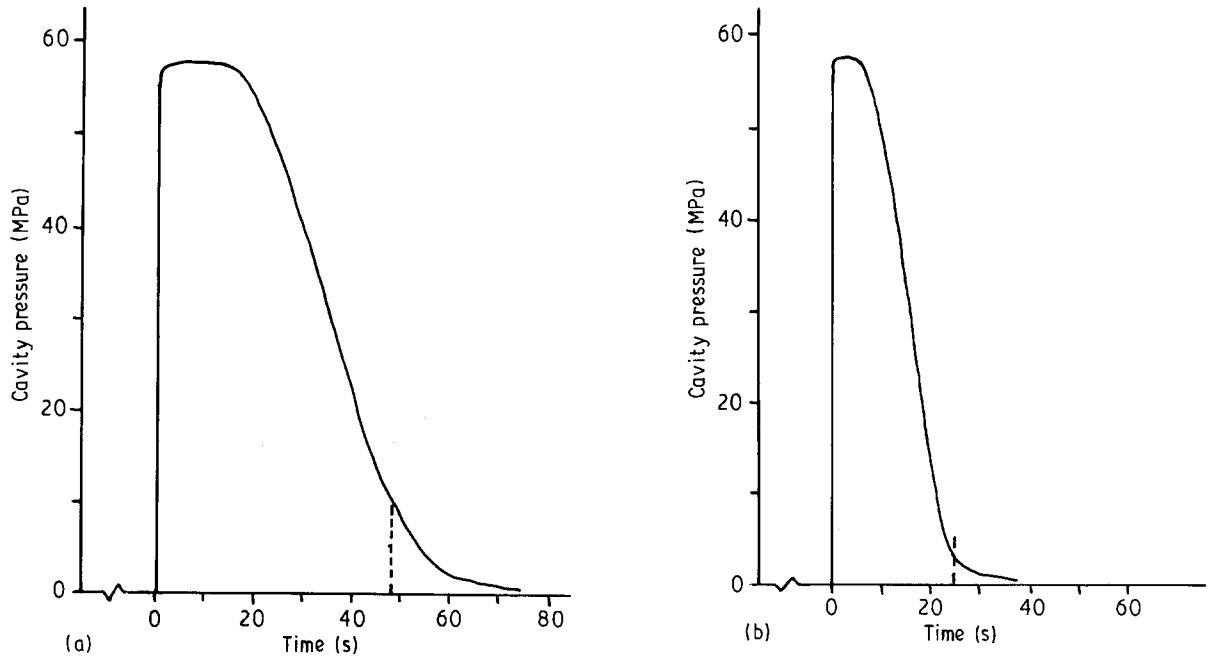

Figure 3 Cavity pressure as a function of time for bars moulded at 493 K to give an initial pressure of 58 MPa with (a) 5 mm and (b) 3.5 mm radius sprue.

4. Results and discussion

4.1. Comparison between cavity pressure fall-off time and sprue solidification time

Fig. 3a and b are typical cavity pressure traces using an injection temperature of 493 K, a mould temperature of 298 K and sprue radii of 5 and 3.45 mm, respectively. The calculated sprue solidification times of 48 and 25 sec are marked on the figures. It is difficult to define a precise time at which cavity pressure begins to fall from the cavity pressure traces; however, the calculated times are clearly much greater than the 15 and 5 s observed in Fig. 3.

This discrepancy has two possible explanations; either the sprue solidifies much sooner than predicted, or the pressure begins to fall before the centre of the sprue becomes solid. The calculated sprue solidification time is based on the measured glass transition temperature (T_g) of 58 °C [9]. The main source of error is that T_g increases with pressure on a material [18]. A reasonable estimate of the increase is 16 °C at a pressure of 50 MPa; this would shorten solidification time by 8 s for the larger sprue, which would not account for the discrepancy.

The latter explanation implies a failure of flow of material through the centre channel of the sprue to compensate for shrinkage in the core of the moulded bar. Since the specific volume varies with temperature and the temperature in the core of mouldings differs from that in the sprue, equations to express the balance of flow were written in terms of mass in the following way:

$$\frac{dM_c}{dt} \leqslant \frac{dM_s}{dt} \quad t \leqslant \text{pressure fall-off time}$$

$$\frac{dM_c}{dt} > \frac{dM_s}{dt} \quad t > \text{pressure fall-off time} \tag{13}$$

where dM_c/dt is the mass flow rate needed to compensate for the change in specific volume of the material in the core of the moulded rectangular bar as the temperature falls, and dM_s/dt is the mass flow rate of material through the sprue. The radius of the fluid region in the sprue falls as material solidifies and the viscosity of the fluid increases, until the rate of flow of material through the sprue is no longer sufficient to compensate for the change in specific volume of material in the molten core of the moulding. The cavity pressure then decreases.

4.2. Prediction of cavity pressure decay

Using the calculation procedure described in Section 3.4, the fall in cavity pressure as a function of time for a fixed sprue closure time of 15 s predicted for a moulding made with an injection pressure of 47 MPa and a sprue radius of 5 mm. This prediction can be compared directly with experiment and the resulting two curves are shown in Fig. 4.

The predicted cavity pressure decays in the same manner as the temperature as expected from consideration of the Spencer and Gilmore equation of state [9], since at constant specific volume the pressure is proportional to the temperature. However, the measured cavity pressure decays more gradually in the initial stage.

Since the start of the decay was taken from the experimental curve it suggests that material continues to fill the mould after 15 s in order to keep the measured cavity pressure higher than predicted, but that flow is insufficient to maintain the original pressure of 47 MPa. This prolonged cavity pressure was observed despite the fact that the wall of the moulded bar was solidifying as cooling proceeded, which would tend to reduce the efficiency of pressure transmission from the molten core to the force transducer pin set in the metal mould. In fact the wall of the

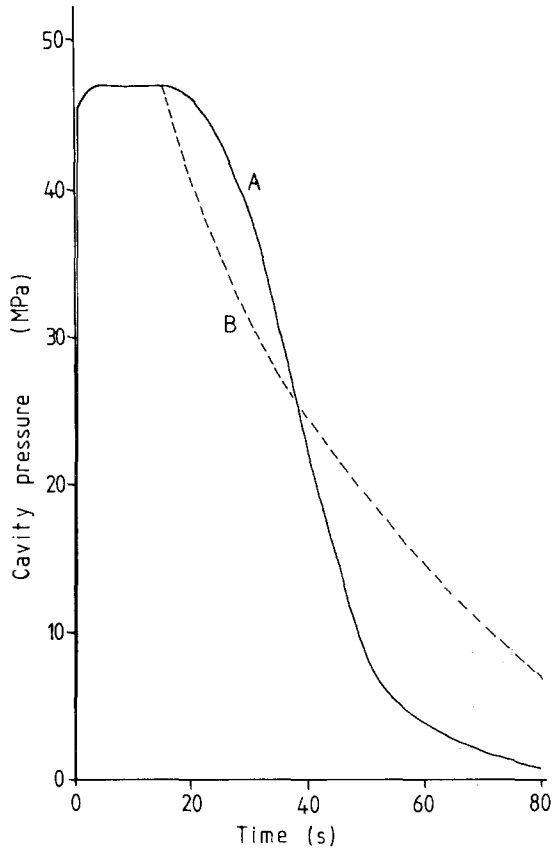

Figure 4 (A) Experimental and (B) calculated cavity pressure decay curves for a moulding with an initial cavity pressure of 47 MPa.

moulding was predicted [10] to solidify after 20 s, which is 5 s after the onset of cavity pressure decay.

The predicted curve uses the average specific volume in the molten pool at the sprue closure time and the equation of state to calculate the subsequent pressure, and is therefore most accurate in the initial stages of solidification. The approximations render the latter stages of the predicted curve less accurate. Furthermore, measured cavity pressure ceases to reflect the pressure in the molten core as solidification of the wall proceeds. The latter stages of the curves cannot, therefore, be compared.

Since the heat flow in both the moulding and sprue can be predicted and the equation of state of the composite is known, Equations 1 and 2 can be tested quantitatively if the rheological properties of the blend are known.

4.3. Calculation of mass flow rates

By obtaining rheological data for the material, it was possible to test the hypothesis that the decay of pressure in the cavity of mouldings was due to a gradual failure of mass transport through the sprue bush. This calculation was performed for a rectangular bar moulded with an initial cavity pressure of 47 MPa using a 5 mm radius sprue bush, by calculating the left- and then the right-hand sides of Equation 13 in turn.

The mass flow rate required to maintain a constant cavity pressure of 47 MPa was obtained by the procedure given in Section 3.3. This rate is plotted in Fig. 5 at 5 s intervals after injection.

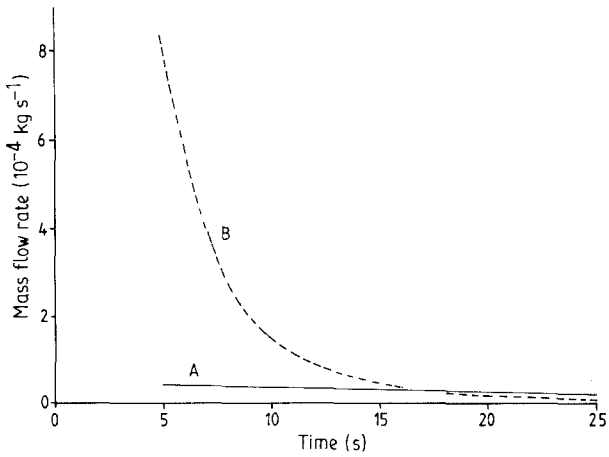

Figure 5 (A) Comparison of mass flow rate needed to compensate for shrinkage of the core and (B) maximum possible mass flow rate along the sprue obtained from viscosity data.

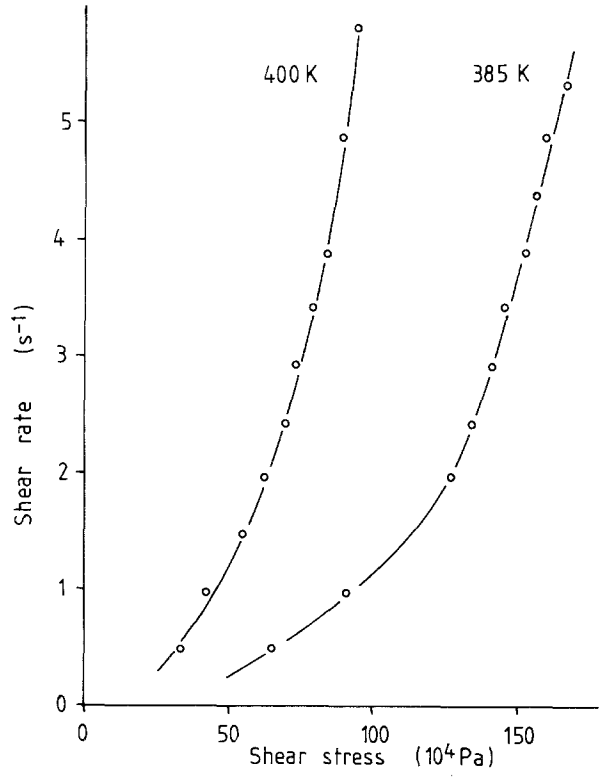

Figure 6 Shear stress against apparent wall shear rate for the suspension at 385 and 400 K.

In order to obtain estimates for the right-hand side of Equation 13, rheological data for the blend were obtained by the method described in Section 2.3. Shear stress against shear rate plots are shown in Figs 6 and 7. Curves for lower temperatures could not be obtained because the viscosity became too high and the equipment was overloaded.

It is well known that the temperature dependence of viscosity of polymers can be expressed by an Arrhenius equation, by the slope $d(\log \eta)/dT$, by free-volume theories or by the Williams–Landel–Ferry equation [19]. Over the temperature range explored in the present work, viscosity data at fixed shear rates were fitted to an Arrhenius equation, and viscosities which could not be measured at low temperatures were

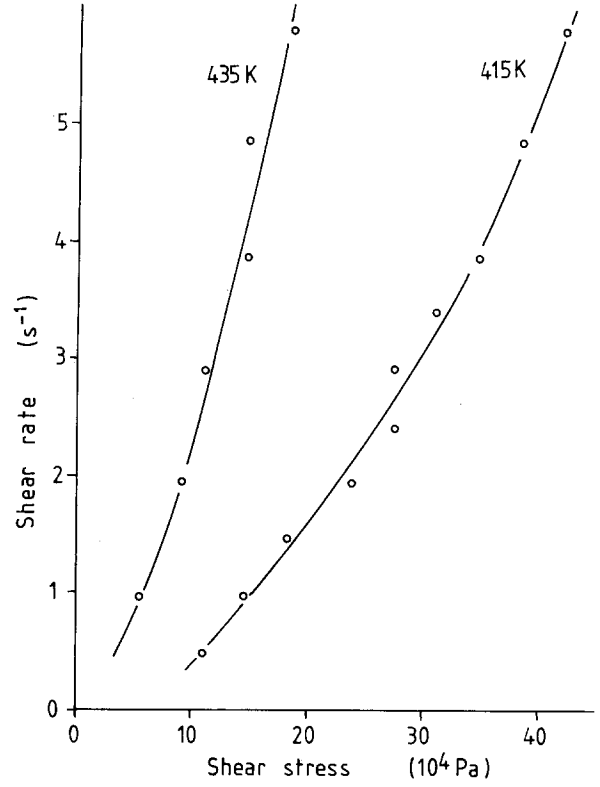

Figure 7 Shear stress against apparent wall shear rate for the suspension at 415 and 435 K.

obtained by extrapolation from 385 K and above down to 366 K.

The shear rate considered in viscosity measurement is the apparent wall shear rate given by [20]

$$\gamma_a = 4Q/\pi r^3 \quad (14)$$

where r is the radius of the capillary and Q is the volume flow rate. Similarly, the wall shear stress is given by [20]

$$\tau = Pr/2l \quad (15)$$

where P is the pressure and l is the length of the capillary.

In modelling the behaviour of material in the sprue, the sprue was taken to be a capillary with a length the same as that of the sprue bush and with a constant radius throughout that length, i.e. the taper was neglected. In defining a radius the problem arises that the flow in the sprue is non-isothermal and a temperature gradient exists across the liquid region, the wall temperature being T_g.

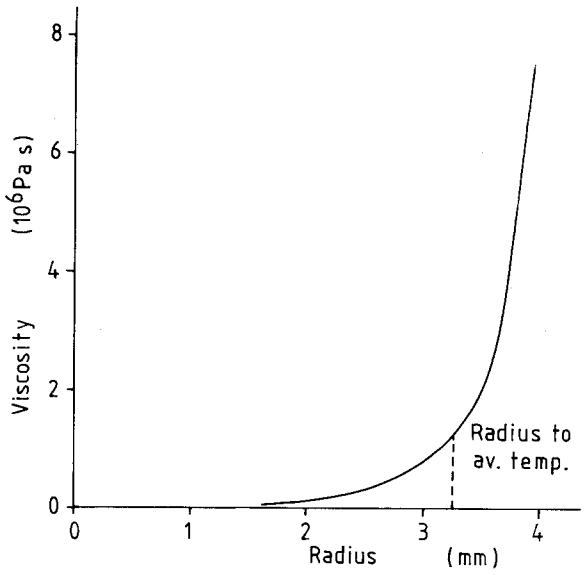

Figure 9 Viscosity of suspension as a function of radius in the 5 mm radius sprue, calculated from the temperature profile of Fig. 8.

A temperature profile for material in the sprue after 15 s is shown in Fig. 8. The volume-average temperature in the fluid region was calculated and an effective radius for flow was defined by taking the distance from the sprue axis to the position corresponding to the average temperature. The shear rate, calculated using the mass flow rate needed to maintain constant pressure in the moulding and the radius just defined, was 0.33 s^{-1} after 15 s. Using this shear rate and the temperature profile of Fig. 8, viscosity against radius data were calculated and are shown in Fig. 9. The shear rate varies with position as does the temperature; however, Fig. 9 shows that taking the radius corresponding to the average temperature is a reasonable approximation.

The flow rates dM/dt calculated by the method in Section 3.3 were used to obtain shear rate values at each 5 s interval by using Equation 14. The viscosity of the composite at these shear rates and at the appropriate average temperatures were then obtained from

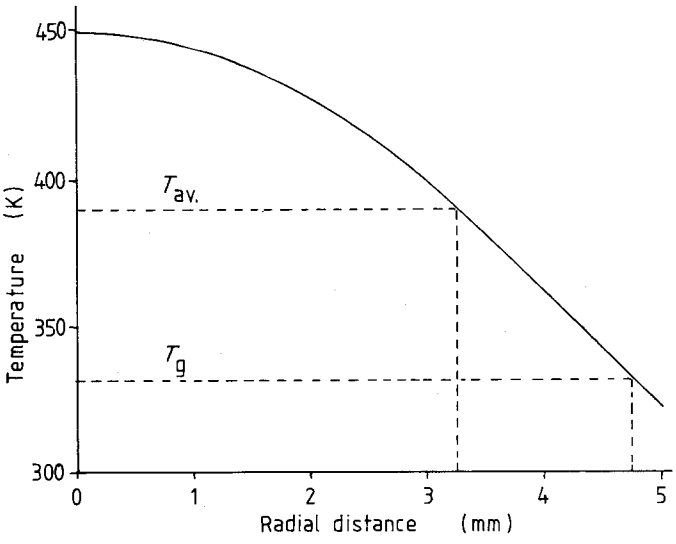

Figure 8 Temperature profile in a 5 mm radius sprue after 15 s, showing the position of the average temperature in the molten region and the position of the glass transition temperature.

the experimental data in Figs 6 and 7. The mass flow rate that was possible through the sprue bush at each time interval was then calculated from Poiseuille's equation [20]:

$$Q = Pr^4/8\eta l \quad (16)$$

Fig. 5 contains plots of flow rate against time required to maintain a constant hold pressure (curve A) and the possible flow rate determined from rheological data (curve B). The cavity pressure may be expected to decrease when the flow rate required to maintain a constant hold pressure becomes greater than the possible flow rate in the sprue. This occurs at approximately 17 s after injection, which agrees well with the 15 s taken from the recorded cavity pressure traces despite the approximations made in order to render tractable a very complex non-isothermal flow problem.

4.4. Consequences of the model

The calculation of flow through the sprue bush as presented here is obviously a gross oversimplification. The temperature of the material varies across the radius of the sprue so that Equations 14, 15 and 16 used to characterize the flow are not strictly valid. Furthermore the heat supplied by mass transport is neglected. However, the calculation does reveal the hypothesis that pressure fall-off is due to a failure of flow to compensate for shrinkage in the core of mouldings to be reasonable, and supports previous empirical statements that a low temperature-dependence of viscosity is a desirable property for ceramic moulding compositions [16].

This theory also explains why using the time at which the cavity pressure just begins to decrease in the prediction of voiding in previous work [10] led to an overestimate of the injection pressure required to achieve a residual pressure greater than zero. Flow does not completely cease at this time and material continues to pack the moulding for a finite time afterwards. Therefore the best estimates that can be achieved by the simulation of voiding presented previously [10] are upper and lower bounds for the injection pressure required to prevent the creation of voids.

5. Conclusions

Sprue closure time is a necessary parameter in modelling the solidification of ceramic injection-moulded bodies, and calculated values deviate significantly from experimentally determined cavity pressure fall times. The final stage of mould packing can be interpreted as a dynamic process in which shrinkage in the cavity demands a mass flow rate along a sprue of diminishing size at decreasing temperature which can no longer be met.

By making simplifications to the complex non-isothermal flow in the sprue, the cavity pressure fall-off time was predicted in terms of the demanded and supplied mass flow. The complexity of the problem means that upper and lower bounds can be obtained for sprue closure time, but the notion of a single point in time where the sprue closes is not correct.

Acknowledgements

The authors are grateful to SERC for supporting this programme and to T & N Technology for donating the powder.

References

1. M. S. THOMAS and J. R. G. EVANS, *Br. Ceram. Trans. J.* **87** (1988) 22.
2. M. J. EDIRISINGHE and J. R. G. EVANS, *J. Mater. Sci.* **22** (1987) 2267.
3. *Idem., Int. J. High Tech. Ceram.* **2** (1986) 249.
4. P. S. ALLAN, M. J. BEVIS, M. J. EDIRISINGHE, J. R. G. EVANS and P. R. HORNSBY, *J. Mater. Sci. Lett.* **6** (1987) 165.
5. M. J. EDIRISINGHE and J. R. G. EVANS, *Mater. Design* **8** (1987) 284.
6. *Idem., ibid.* **9** (1988) 85.
7. J. G. ZHANG, M. J. EDIRISINGHE and J. R. G. EVANS, *J. Euro. Ceram. Soc.* **5** (1989) 63.
8. *Idem., J. Mater. Sci.* **24** (1989) 840.
9. K. N. HUNT, J. R. G. EVANS and J. WOODTHORPE, *J. Mater. Sci.*, in press.
10. *Idem., ibid.*
11. J. A. BRYDSON, "Flow Properties of Polymer Melts" (Iliffe, London, 1970) p. 100.
12. I. I. RUBIN, "Injection Moulding Theory and Practice" (Wiley, New York, 1972) p. 275.
13. M. R. KAMAL and S. KENIG, *Polym. Eng. Sci.* **12** (1972) 294.
14. *Idem., ibid.* **12** (1972) 302.
15. D. HUILIER, C. LENFANT, J. TERRISSE and R. DETERRE, *ibid.* **28** (1988) 1637.
16. M. J. EDIRISINGHE and J. R. G. EVANS, *Br. Ceram. Trans. J.* **86** (1987) 18.
17. B. CARNAHAN, H. A. LUTHER and J. O. WILKES, "Applied Numerical Methods" (Wiley, New York, 1969) pp. 441–442.
18. M. C. SHEN and A. EISENBERG, in "Progress in Solid State Chemistry", Vol. 3, edited by H. Reiss (Pergamon, Oxford, 1966) p. 456.
19. J. A. BRYDSON, "Flow Properties of Polymer Melts" (Iliffe, London, 1970) pp. 47–50.
20. *Idem., ibid.* pp. 21–30.

Received 6 December 1989
and accepted 23 July 1990